Accuracy of Fiber Propagation Evaluation Using Phenomenological Attenuation and Raman Scattering Models in Multiband Optical Networks

Nanostructuring of HighTC Superconductors into MicroSized Zones

E. Mezzetti, D. Botta, A. Chiodoni, R. Gerbaldo, G. Ghigo et al.

Citation: AIP Conf. Proc. **824**, 786 (2006); doi: 10.1063/1.2192424
View online: http://dx.doi.org/10.1063/1.2192424
View Table of Contents: http://proceedings.aip.org/dbt/dbt.jsp?KEY=APCPCS&Volume=824&Issue=1
Published by the American Institute of Physics.

NANOSTRUCTURING OF HIGH-T_C SUPERCONDUCTORS INTO MICRO-SIZED ZONES.

E. Mezzetti[1], D. Botta[1], A. Chiodoni[1], R. Gerbaldo[1], G. Ghigo[1], L. Gozzelino[1], F. Laviano[1], B. Minetti[1], A. Rovelli[2], A. Amato[2], R. Cherubini[3]

[1] INFN-Sez Torino; Dep. Of Physics, Politecnico di Torino, c.so Duca degli Abruzzi, 24; 10124 Torino, Italy

[2] INFN-LNS, Catania, Italy

[3] INFN-LNL, Legnaro (Padova), Italy

ABSTRACT

A special apparatus was designed in order to "write", with nanometric resolution, microsize-confined nanostructures in oxide samples. The nanostructures are produced by high energy heavy ion irradiation that allows nanostructuring the sample over its full thickness. The properties of the nanostructured areas can be further modulated by choosing the proper energy and fluence of the incoming ion beam. We present this set-up and different kinds of nanostructured patterns created on high temperature superconducting films. We used the magneto-optical analysis to directly show the effect of the confined nanostructures on the micron scale. The confined nanostructured area, embedded in the virgin matrix, is demonstrated to be a fruitful element for designing a new class of devices.

KEYWORDS: High-temperature superconductors; High-energy heavy-ion irradiation; Confined Nanostructuring
PACS: 74.25.Qt, 74.25.Sv, 85.40.-e

INTRODUCTION

High Energy Heavy Ion (HEHI) irradiation has been widely used to increase the pinning capabilities of superconductors, especially high temperature superconductor specimens [1].

The HEHI irradiation exhibits many advantages over other kinds of nanostructuring techniques (even keV irradiation [2]): the defect density, very often measured as a matching equivalent field B_Φ, can be accurately determined, the defect size is optimally matching with the coherence length of high temperature superconducting materials [3] and the shape is well correlated along the irradiation direction. These defects (called columnar defects – CD's), allow a three dimensional (3D) modulation of the vortex pinning by tilting

CP824, *Advances in Cryogenic Engineering: Transactions of the International Cryogenic Materials Conference - ICMC, Vol. 52,* edited by U. Balachandran

the vortex direction with respect to the CD one [4]. The capability to modulate the vortex pinning through introduction of micrometric size periodic structures by HEHI lithography has recently be demonstrated [5]. The micrometric modulation provides a valuable tool for studying the vortex matter behaviour into confined geometries [6] and, in turns, for controlling both the pinning [7] and the screening capabilities of the superconducting system in a reliable way, i.e., to modulate both Meissner and critical currents. In dependence on the irradiation energy, which determines the implantation depth into the substrate, and on the fluence the superconducting properties can be easily enhanced or depressed. Because of the strong intrinsic pinning of the superconducting oxide films, a depression of the pinning potential would be very effective for obtaining sharp current modulation in a stronger superconducting matrix. Therefore, the local modulation can be exploited for confining external perturbation as a local dissipative state generated in an irradiated region.

Following these ideas, we developed two tailored protocols for producing the micrometric size modulation: laser-cut metal mask as fixed micro-collimators [8] (at the Tandem facility, INFN-LNL) and a novel apparatus that allows the 2D movement of the confined HEHI beam on the sample surface with nanometric resolution [9] (at the Superconducting Cyclotron facility, INFN-LNS). In this way, we are able to pattern any kind of micrometric size geometries, included also not simply connected regions. Here, we briefly present the irradiation apparatus, some irradiation geometries, and the basic slit geometry used as a local magnetic field detector. The paper is organized as follows. The experimental set-ups for micro-collimated irradiations are described in Section 2. In this section, the issues of beam calibration and local fluence evaluation are addressed. In Section 3, "writing" of micropatterns of any programmed shape is demonstrated. Then, a single nanostructured region is presented as a local magnetic field detector.

EXPERIMENTAL APPARATUS

The HEHI beam is confined by means of laser-cut stainless steel masks, with a pinhole or a slit of micrometric size. The micrometric aperture lateral size depends on the mask thickness, e.g., for a 150 μm thick masks we obtained a 30 μm diameter pinhole. The thickness of the mask has to be chosen in dependence on the HEHI energy, for stopping the incoming ions outside the micrometric aperture. These masks can be directly fixed on the sample holder, over the sample surface, after the alignment under an optical microscope (INFN-LNL).

For generating complex patterns, such as not simply connected geometries, a dedicated in-vacuum irradiation apparatus was designed at INFN-LNS [9]. In Figure 1, the schematic drawing of the experimental set-up of this apparatus is shown. The basic components are two cross-mounted MICOS Linear Stages LS-110 (Fig. 1, n.7) which control the bi-directional movement of the target in a plane perpendicular to the HEHI direction. Optical encoders and motor controller electronics Micos SMC Taurus enable the target to be moved with a resolution of 15 nm over a total length of 28 mm. The target and a scintillating screen (Fig. 1, n.4) are positioned on a sample holder of transparent lead glass (Fig. 1, n.5). A CCD camera is positioned close to the backside of the sample holder and is centered with respect to the HEHI direction (Fig. 1, n.6), in order to visualize the HEHI spot hitting the scintillating screen. The irradiation-fluence is measured by a suitably assembled Faraday Cup (henceforth labeled FC#1).

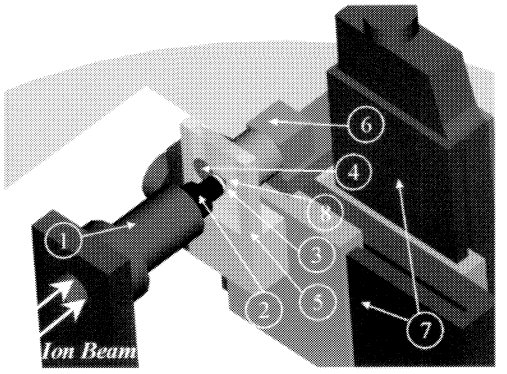

FIGURE 1. Schematic drawing of the experimental arrangement of the irradiation set up for high-energy heavy-ion patterning: (1) Faraday Cup #1 – (2) Small size cylinder – (3) Stainless steel disk with micrometric pinhole aperture – (4) Scintillating screen – (5) Lead-glass sample holder – (6) CCD camera – (7) Linear stages – (8) Sample.

Another Faraday Cup (henceforth labeled FC#2) positioned upstream the apparatus is used as a shutter as well as a reference for beam current evaluation. The FC#1 has a threaded hole (Ø 15 mm) at the bottom. A stainless steel cylinder closed by a micrometric pinhole can be screwed to the FC#1 in order to act as micro-collimator (Fig. 1, n.3). Both the Faraday Cups are connected to an electronic apparatus with two input channels: the first one is a current/voltage converter used for reading the reference FC#2, the second one is a charge/pulse converter (1 pC/pulse), used for integrating the HEHI current during the irradiation, see Figure 2. The typical beam current for the irradiation is lower than 1 nA. The electronic board is connected with a NI-PCI 6024E DAQ board installed into the local PC that also drives the motor controllers.

The first step for the beam calibration is a tuning procedure aimed at achieving a suitable homogeneity of the HEHI beam profile. During this operations, the micro-collimator is removed and the beam distribution is studied by the profiles visualized by the CCD camera.

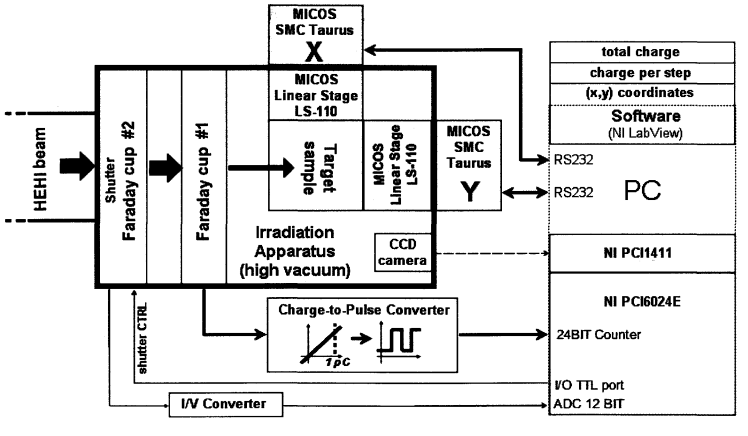

FIGURE 2. Block diagram of the main electronic components of the irradiation apparatus.

Once optimal beam conditions are steadily obtained, the microcollimator is screwed on the bottom of FC#1. The HEHI beam passing through the pinhole aperture hits the scintillating screen and is visualized by the CCD camera. The user, by means of the camera zoom, can control the alignment of the beam with respect to the sample position.

In order to evaluate the irradiation fluence hitting the sample, ϕ, we first measure the two-dimensional charge probability density function $f(x, y)$ from the HEHI beam profile. Then the relation between q_{hole} (charges crossing the microcollimator) and the total released charge q_{tot} is:

$$\frac{q_{hole}}{q_{tot}} = \iint_{hole} f(x,y)dxdy \tag{1}$$

and:

$$\phi = q_{hole}/(n \cdot e \cdot A) \tag{2}$$

where n is the ion charge, e is the elementary charge and A is the pinhole aperture area.

The apparatus allows one to measure the HEHI current inside the FC#1 and the total charge, q_{FC1}, released onto it. Therefore $q_{\text{tot}} = q_{\text{FC1}} + q_{hole}$, and the relation between q_{FC1} and q_{hole} results to be:

$$q_{hole} = q_{FC1}\left(\frac{\iint_{hole} f(x,y)dxdy}{1-\iint_{hole} f(x,y)dxdy}\right) \tag{3}$$

It turns out that q_{hole} is about 0.2% of q_{FC1} for a 70 μm pinhole aperture and becomes about 0.04 % for a 30 μm pinhole aperture.

After the beam calibration, the nanostructured patterns are obtained by giving a user defined coordinate set to the control software. To increase the smoothness of the drawn patterns, each couple of x-y coordinates can cover a fraction of the pinhole aperture diameter (due to the nanometric resolution of the movement stage). The dose to be released, step by step, is also chosen by the user; therefore, inside the nanostructured pattern, any dose profile can be obtained [10]. For a more detailed description of this equipment see [9].

RESULTS AND DISCUSSION

High temperature superconducting $YBa_2Cu_3O_{7-x}$ (YBCO) films were grown by means of thermal co-evaporation technique on yttria stabilized zirconia (YSZ) substrate, with a 40 nm thick CeO_2 buffer layer [11]. The critical current density is over 10^{11} A/m^2 at T = 4.2 K. All the films here presented are 300 nm thick.

The HEHI beam was always directed perpendicular to the film surface, so CD's are parallel to the YBCO c-axis. Au-ions cross the YBCO film (and the CeO_2 buffer layer), and implant in the YSZ substrate. The energy released by the ions is almost constant along the whole YBCO film thickness and is high enough to induce columnar tracks, even at 250 MeV [12]. The implantation of the ions into the substrate leads to a feedback stress toward the YBCO film that depends on the depth of implantation, i.e., on the HEHI energy. For a given energy, there is a threshold fluence corresponding to the crossover between enhancement and depletion of the pinning properties, thus we can completely modulate the superconducting capabilities through the defect density and the released dose.

Direct visualization of the effects of confined nanostructuring into superconducting films is achieved by the magneto-optical analysis [13,14,15]. The magneto-optical signal is obtained by coupling the superconductor with a ferromagnetic indicator film that rotates the polarization plane of an incident light beam in dependence on the local magnetic field.

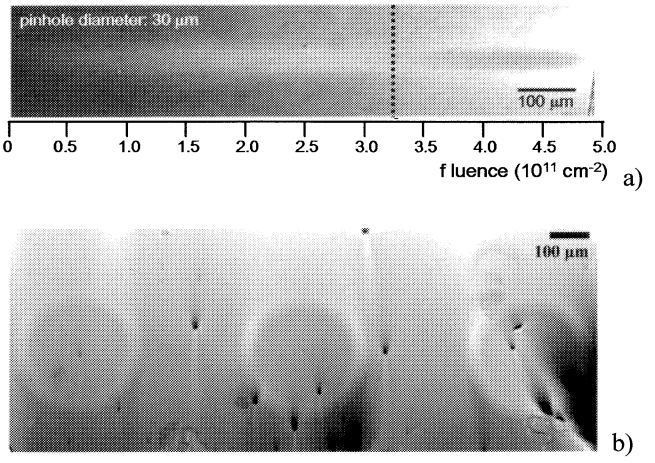

FIGURE 3. a) Nanostructured linear gradient on YBCO film: the irradiation fluence increases from left to right. The image is taken in remnant state after a field cooling in a magnetic field of 90 mT at T = 40 K. The damage threshold is at a fluence of about $3.25 \cdot 10^{11}$ ion/cm^2 (4.2 GeV Au ions). As the fluence increases the pinning strength increases too (left side of the figure) until at higher fluences, above the dotted line (crossover fluence), the dark zone is less able to pin the vortices and is permanently damaged. b) Magneto-optical images of another YBCO sample after ion patterning with ring geometries. These patterns were obtained by means of 4.2 GeV Au-ions ($\phi = 1.0 \cdot 10^{11}$ ion/cm^2) by collimating the ion beam through a circular 70 μm large pinhole. The images were taken at T = 50 K in remnant state after a field cooling in a magnetic field of 80 mT. Brighter gray levels: higher magnetic flux density regions (higher remnant magnetic field), darker grey levels: lower magnetic flux density regions.

The local polarization modulation can be imaged in real-time over the whole sample surface and can be converted into quantitative magnetic field and supercurrent values [16].

In Figure 3, the magneto-optical images of different pattern geometries (a linear dose gradient and several rings) are reported. The linear gradient displays the above mentioned crossover threshold, corresponding to about $3.25 \cdot 10^{11}$ ion/cm^{-2}, for 4.2 GeV Au ions.

Inside the superconducting condensate, these patterns behave as macroscopic defects [17]. Many features, which are typical of the nonlinear electrical current flow, e.g., the characteristics magnetic flux jets starting from the nanostructured pattern edges and pointing toward the sample center, are well visible in the ring patterns. They indeed reveals long range disturbances of the normal component of B(x,y) due to the interaction of vortices and screening currents with the whole ensemble of CD's.

In Figure 4, an infinite-shaped nanostructured area was created in a disk patterned sample, in order to measure the local supercurrent density [16]. The irradiation fluence was chosen in such a way to deeply inhibit the critical currents, since, as said above, the YBCO film already shows very strong pinning capabilities. The irradiation pattern is very evident and the vortex distribution resembles its shape. The current density distribution shows that the critical current was sharply modified with respect to the pristine part. Moreover, the local current density inside the irradiated area is further modulated by the vortex position outside the pattern (due to the long-range disturbance). In the center of the irradiated region, a depleted critical current surprisingly corresponds to a high vortex density. All these effects can be suitably controlled by changing the pattern geometry [18].

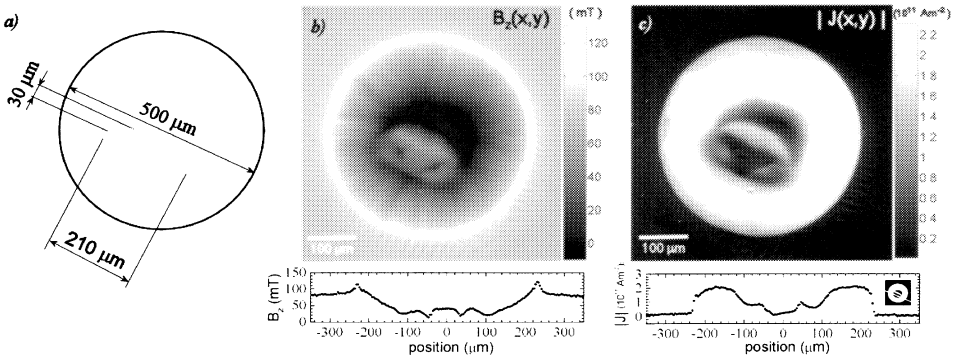

FIGURE 4. a) Scheme of the sample with the "infinite" like pattern. b) Magnetic field (z component) over the YBCO sample surface at T = 5 K with an applied magnetic field of 78.3 mT, after zero field cooling. The profile below is traced on the same location shown in the inset of the graph in c). The nanostructured pattern was created with a HEHI beam confined in 30 μm ($5 \cdot 10^{11}$ ion/cm^2, 4.2 GeV Au ion). c) Current density modulus distribution corresponding to the magnetic field map shown in b).

The possibility to strongly modulate the superconducting properties without any other deposition or chemical process, allows us to design local nanostructured regions that act as local detectors for an external perturbation. Namely, if the local superconducting properties are depleted (without completely destroying the superconducting state and leaving untouched the sample shape), the whole sample can be electrically biased at a temperature where the nanostructured region is in the so-called "flux-flow" state, while the remaining part are in the "vortex glass" phase. In this way, the vortices can freely move only in the nanostructured region and their movement, under the action of a transport current, will produce a dissipative signal only across it.

A magneto-optical picture, Figure 5(a), demonstrates the depleted pinning capabilities of the nanostructured region, although still superconducting. This effect is schematically drawn in Figure 5(b).

In this configuration, an external magnetic field can be locally detected and measured as the vortices are freely generated and move across the nanostructured pattern. The voltage drop can be easily tuned by changing the temperature in the neighborhoods of the transition temperature, see Figure 6, where it is presented a 4-contacts transport measurement in increasing and decreasing magnetic field.

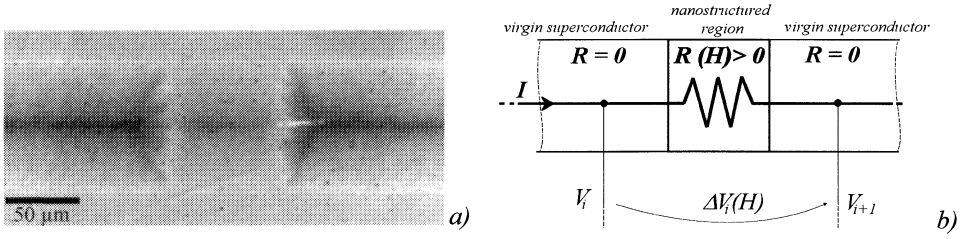

FIGURE 5. a) Magneto-optical image of a YBCO strip, nanostructured with a slit of 70 μm. The region, corresponding to the center of the image, was irradiated with a fluence of 10^{11} ion/cm^2 (250 MeV Au ion). The image was taken at T = 70.3 K, with an applied field of 50 mT. The reduction of the pinning capabilities and the increased vortex mobility are evident from the much softer critical gradient. The dissipative effect of the interfaces is also clearly visible. b) Scheme of the electrical behaviour of such a nanostructured strip in presence of an applied magnetic field, under an electrical bias.

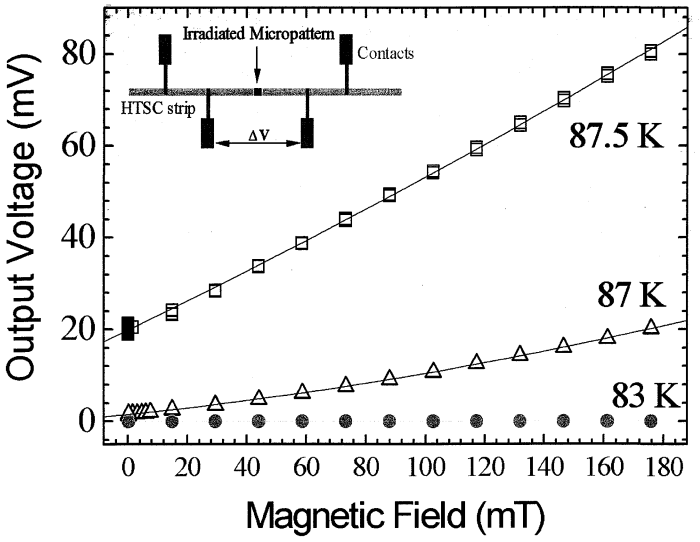

FIGURE 6. Transport measurement of the nanostructured YBCO strip (see Figure 5), in increasing and decreasing magnetic field (points overlap), at different temperatures and for I= 5 mA. For the shown range of temperatures and applied magnetic fields, the virgin part of the sample does not contribute to the measured signal (its T_c is around 90.5 K).

CONCLUSIONS

We presented a thorough approach for confined nanostructuring of oxide films. The basic approach consists into confining the HEHI beam in a micrometric size spot, then a special apparatus was designed in order to produce any kind of drawing on the sample surface, with nanometric resolution. The properties of the nanostructured areas can be further modulated by choosing the proper energy and fluence of the incoming HEHI beam.

We demonstrated the feasibility and the powerful use of this set-up by producing different kinds of nanostructured patterns on high temperature superconducting films. The confined nanostructured area is then shown to be a fruitful element for designing a new class of devices. In particular, we demonstrated that a simple pattern can be readily used for a local magnetic field detector.

ACKNOWLEDGMENTS

We acknowledge the contribution of the Istituto Nazionale di Fisica Nucleare (I.N.F.N.) under the Di.S.Co.L.I. project.

REFERENCES

1. Hensel, B., Roas, B., Henke, S., Hopfengartner, R., Lippert, M., Strobel, J. P., Vildic, M., Saemann-Ischenko, G. and Klaumunzer, S., *Phys. Rev. B* **42**, 4135 (1990); Civale, L., Marwick, A. D., Worthington, T. K., Kirk, M. A., Thompson, J. R., Krusin-Elbaum, L., Sun, Y., Clem, J. R. and Holtzberg, F., *Phys.*

Rev. Lett. **67**, 648 (1991); Konczykowski, M., Rullier-Albenque, F., Yacoby, E. R., Shaulov, A., Yeshurun Y. and Lejay, P., *Physica C* **185-189**, 2347 (1991); Budhani, R.C., Suenaga, M., Liou, S.H., *Phys. Rev. Lett.* **69**, 3816 (1992).
2. Tinchev, S.S., *Supercond Sci. Technol.* **3**, 500 (1990).
3. Blatter, G., Feigel'man, M. V., Geshkenbein, V. B., Larkin, A. I. and Vinokur, V. M., *Rev. Mod. Phys.* **66**, 1125 (1994).
4. Silhanek, A. V., Civale, L. and Avila, M. A., *Phys. Rev. B* **65**, 174525 (2002); Mikitik, G. P. and Brandt E. H., *Phys. Rev. B* **62**, 6800 (2000); Laviano, F., Botta, D., Chiodoni, A., Gerbaldo, R., Ghigo, G., Gozzelino, L. and Mezzetti, E., *Phys. Rev. B* **68**, 014507 (2003).
5. Kwok, W. K., Olsson, R. J., Karapetrov, G., Welp, U., Vlasko-Vlasov, V., Kadowaki, K. and Crabtree, G. W., *Physica C* **382**, 137 (2002).
6. Marchetti, M. C. and Nelson, D. R., *Phys. Rev. B* **59**, 13624 (1999); Banerjee, S. S., Soibel, A., Myasoedov, Y., Rappaport, M., Zeldov, E., Menghini, M., Fasano, Y., de la Cruz, F., van der Beek, C. J., Konczykowski, M. and Tamegai, T., *Phys. Rev. Lett.* **90**, 087004 (2003); Zhu, B. Y., Marchesoni, F., Moshchalkov, V. V. and Nori, F., *Phys. Rev. B* **68**, 014514 (2003).
7. Mezzetti, E., Gerbaldo, R., Ghigo, G., Gozzelino, L., Minetti, B., Camerlingo, C., Monaco, A., Cuttone, G. and Rovelli, A., *Phys. Rev. B* **60,** 7623 (1999).
8. Mezzetti, E., Laviano, F., Botta, D., Chiodoni, A., Gerbaldo, R., Ghigo, G., Gozzelino L., in "Magneto-optical Imaging" edited by T.H. Johansen and D.V. Shantsev, NATO Science Series, Kluwer Academic Publishers, The Netherlands, 197 (2004).
9. Rovelli, A., Amato, A., Botta, D., Chiodoni, A., Gerbaldo, R., Ghigo, G., Gozzelino, L., Laviano, F., Minetti, B. and Mezzetti, E., *Nuclear Inst. and Methods in Physics Research B*, in press.
10. Ghigo, G., Botta, D., Chiodoni, A., Gerbaldo, R., Gozzelino, L., Laviano, F., Minetti, B., Mezzetti, E. and Andreone, D., *Supercond. Sci. Technol.* **17**, 977 (2004).
11. Utz, B., Semerad, R., Bauer, M., Prusseit, W., Berberich, P. and Kinder, H., *IEEE Trans. Appl. Supercond.* **7**, 1272 (1997).
12. Hardy, V., Provost, J., Groult, D., Simon, Ch., Hervieu, M. and Raveau, B., *J. Alloys Compd.* **195** (1993) 395.
13. Koblischka M. R. and Wijngaarden, R. J., *Supercond. Sci. Technol.* **8**, 199 (1995).
14. Polyanskii, A. A., Feldmann, D. M. and Larbalestier, D.C., Handbook of Superconducting Materials (Bristol: Institute of Physics Publishing) (1999) appendix C.3.4.
15. Jooss, Ch., Albrecht, J., Kuhn, H., Leonhardt, S., Kronmuller, H., *Rep. Prog. Phys.* **65,** 651 (2002).
16. Laviano, F., Botta, D., Chiodoni, A., Gerbaldo, R., Ghigo, G., Gozzelino, L., Mezzetti, E. and Zannella, S., *Supercond. Sci. Technol.* **16,** 71 (2003) and references therein.
17. Gurevich, A. and Friesen, M., *Phys. Rev. B* **62**, 4004 (2000).
18. Brandt, E. H., *Phys. Rev. B* **64**, 024505 (2001).